

Ultrafast laser generated strain in granular and continuous FePt thin films

A. von Reppert,¹ L. Willig,¹ J.-E. Pudell,¹ M. Rössle,² W. Leitenberger,¹ M. Herzog,¹
 F. Ganss,³ O. Hellwig,^{3,4} and M. Bargheer^{1,2,a)}

¹Institut für Physik und Astronomie, Universität Potsdam, Karl-Liebknecht-Str. 24-25, 14476 Potsdam, Germany

²Helmholtz-Zentrum Berlin für Materialien und Energie GmbH, Wilhelm-Conrad-Röntgen Campus, BESSY II, Albert-Einstein-Str. 15, 12489 Berlin, Germany

³Institut für Physik, Technische Universität Chemnitz, Reichenhainer Str. 70, 09126 Chemnitz, Germany

⁴Institut für Ionenstrahlphysik und Materialforschung, Helmholtz-Zentrum Dresden-Rossendorf, Bautzner Landstrasse 400, 01328 Dresden, Germany

(Received 28 July 2018; accepted 2 September 2018; published online 18 September 2018)

We employ ultrafast X-ray diffraction to compare the lattice dynamics of laser-excited continuous and granular FePt films on MgO (100) substrates. Contrary to recent results on free-standing granular films, we observe in both cases a pronounced and long-lasting out-of-plane expansion. We attribute this discrepancy to the in-plane expansion, which is suppressed by symmetry in continuous films. Granular films on substrates are less constrained and already show a reduced out-of-plane contraction. Via the Poisson effect, out-of-plane contractions drive in-plane expansion and vice versa. Consistently, the granular film exhibits a short-lived out-of-plane contraction driven by ultrafast demagnetization which is followed by a reduced and delayed expansion. From the acoustic reflections of the observed strain waves at the film-substrate interface, we extract a 13% reduction of the elastic constants in thin 10 nm FePt films compared to bulk-like samples. © 2018 Author(s). All article content, except where otherwise noted, is licensed under a Creative Commons Attribution (CC BY) license (<http://creativecommons.org/licenses/by/4.0/>). <https://doi.org/10.1063/1.5050234>

The L1₀ ordered phase of FePt is a prominent example of a highly anisotropic material with a simple unit cell, which can be easily stabilized in nanoscale thin films.^{1,2} Its technological relevance originates from the large uniaxial magnetic anisotropy (K_u),^{2,3} which makes FePt the material of choice for heat-assisted magnetic recording (HAMR) schemes.^{4,5} Established bulk characterization methods for thermophysical properties, i.e., elastic constants (C_{ij}), heat capacity (C_p), thermal conductivity (κ), and thermal expansion coefficients (α), are mostly inapplicable in such nanoscale thin film materials. The envisioned applications nevertheless substantiate the need for a thorough characterization of all involved properties.

Ideally, the inaccessible properties of the material could be calculated on an *ab-initio* basis. The so far simulated properties relevant to the HAMR process range from the Curie temperature variation in granular films^{6,7} over *ab-initio* models for mode specific electron phonon coupling constants⁸ up to full multiscale models for the magnetization dynamics.⁹ Apart from recent mode specific calculations of the phonon Grüneisen constants¹⁰ (Γ) and extensive work on the elastic constants,¹¹⁻¹³ predictions for C_p , κ , and α are lacking, which hints at the complexity of full *ab-initio* theoretical approaches.

Experimental methods tailored to be applicable in the thin-film regime have been developed alongside the improved thin film growth techniques. Specifically, for FePt, time-domain thermoreflectance in combination with 1D thermal transport models has been used to extract the heat conductivity and thermal boundary resistances.^{14,15} Even an estimate for the diverging magnetic specific heat

has been obtained.¹⁶ The out-of-plane elastic constant C_{33} has been determined by picosecond ultrasonics from the coherent phonon propagation monitored by an all-optical pump-probe method¹⁷ and electromagnetic-acoustic resonance.¹⁸ Diffraction studies on L1₀ FePt compounds report a strong anisotropy in the thermal expansion upon equilibrium heating where the dominant in-plane expansion heralds anisotropic stresses.^{19,20}

A recent time-resolved investigation has combined the direct access to the structural dynamics of FePt nanograins via ultrafast electron diffraction (UED) with direct measurements of the Fe magnetization by resonant soft X-ray diffraction.¹⁰ This study connected the obtained experimental interpretation with the insight of *ab-initio* theory to study the complex coupled dynamics initiated by the simultaneous action of electronic, magnetic, and phononic stress contributions.¹⁰ The ultrafast demagnetization and potentially anisotropic electron and phonon stresses were found to drive a pronounced out-of-plane contraction that decays to zero within 20 ps. For this experiment, the FePt nanograins embedded in a carbon matrix were transferred from the substrate to an ultrathin metal grid suitable for UED and the out-of-plane lattice motion was derived from asymmetric diffraction peaks. Ultrafast X-ray diffraction (UXRD) in the symmetric Bragg reflection geometry is an established method for measurements of the lattice expansion of thin films and heterostructures that are supported by a substrate.^{21,22} A synchrotron-based UXRD study²³ on continuous FePt films has reported an out-of-plane expansion upon photo-excitation; however, the time resolution was insufficient to observe the acoustic vibrations.¹⁰

Here, we present laser-based UXRD experiments on FePt in the L1₀ phase on MgO substrates with a time resolution of approximately 200 fs. We compare the lattice

^{a)}bargheer@uni-potsdam.de

response of a continuous crystalline FePt thin film to the nano-granular FePt samples in a carbon matrix relevant for magnetic recording. Both samples are investigated as-grown onto the MgO (100) substrates. In contrast to the out-of-plane contraction in free-standing granular FePt films, observed by UED in the transmission geometry on a transmission electron microscopy (TEM) grid,¹⁰ we observe an ultrafast out-of-plane expansion within 2.5 ps limited by the sound velocity. From the observed coherent phonon oscillations period of 4.6 ps and a precise measurement of the film thickness $d = 9.7$ nm by X-ray reflectivity (XRR), we derive an out-of-plane longitudinal acoustic sound velocity of 4.2 nm/ps which is in line with the previously reported elastic constants¹⁷ and with the periods observed by UED.¹⁰ We discuss that the out-of-plane structural dynamics strongly varies for different film morphologies because out-of-plane contractions are coupled to in-plane expansion by the Poisson effect. Our study thus illustrates the capabilities of laboratory-based UXRD for determining the elastic constants in ultrathin samples. From a conceptually simple one-dimensional linear chain (LC) model, we furthermore obtain the different stresses that drive the out-of-plane response in granular and thin-film media.

We compare granular and continuous FePt films that are both in the L1₀ phase and grown onto MgO (100) oriented substrates. The continuous film was prepared by magnetron-sputtering Fe and Pt from a composite FePt target onto a substrate preheated to 500 °C. The granular film was sputtered from a FePt-carbon composite target with approximately 30 vol. % C onto a substrate preheated to 650 °C. The *c*-axis and magnetization are oriented out-of-plane. XRR was carried out to characterize the film thicknesses at the KMC3-XPP endstation²⁴ at the BESSY II synchrotron radiation facility. Using programs from the reflpak suite,²⁵ the XRR data in Figs. 1(a) and 1(c) were analyzed and fitted by the resulting electron density depicted in Figs. 1(e) and 1(f). The insets (b) and (d) depict the inferred sample structures. The Kiessig fringes of the granular film decay quickly, confirming the increased surface roughness known from cross sectional TEM images of comparable samples.^{2,26}

Scanning electron microscopy (SEM) images of similarly prepared samples (not shown) display that the granular film consists of segregated FePt-nanograins with a size distribution centered at approximately 10 nm embedded in amorphous carbon that magnetically decouples the grains. This is confirmed by the magnetic hysteresis measurements shown in Fig. 1(g) carried out using a commercial SQUID-vibrating sample magnetometer (Quantum Design). The granular sample exhibits a large coercive field of approximately $\mu_0 H = 5$ T, which is desirable for HAMR, whereas the thin film switches at a considerably reduced field of $\mu_0 H = 0.4$ T via domain wall motion, which is inhibited in granular samples.²⁷ The saturation magnetization for the granular film is reduced by a factor of 0.7 as compared to the continuous film, which agrees with the volume filling factor of FePt in the non-magnetic carbon estimated from SEM images.

Using UXRD, we monitor the Bragg peak shift in the symmetric Bragg diffraction geometry and thus the out-of-plane lattice expansion of the two different crystalline

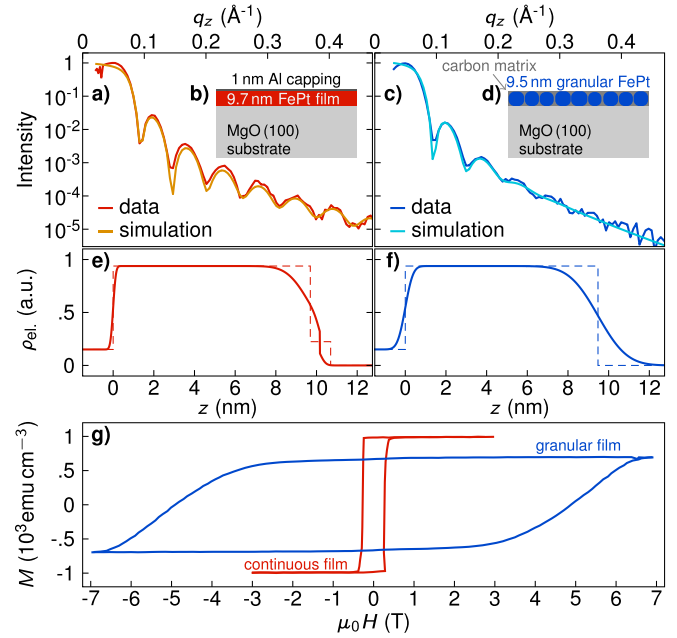


FIG. 1. Sample characterization: X-ray reflectivity data of the continuous (a) and granular (c) film. Orange and cyan colored lines indicate the fit result obtained by assuming the electron densities shown in (e) and (f). Sample structures derived from the electron density without roughness [dashed lines in (e) and (f)] are schematically shown in the insets (b) and (d). The magnetization hysteresis in (g) shows a strongly enhanced coercivity and a reduced saturation magnetization of the granular film compared to the continuous film.

specimens with sub-picosecond time resolution at a laboratory-based diffraction setup.²⁸ Figure 2(a) displays the Bragg diffraction curve of the unexcited granular and continuous film samples and the inset (b) schematically shows the diffraction and pump-probe geometry. The MgO (002) substrate peak is located at $\theta = 21.45^\circ$, and the (002) FePt-peaks appear approximately at $\theta = 24.6^\circ$. We optically excite the samples with *p*-polarized pump pulses with a central wavelength of 800 nm and a pulse duration of 100 fs. From the 0.2 mJ pulse energy at a 1 kHz repetition rate with a 1.4 mm \times 1.5 mm (FWHM) beam profile incident under $\beta = 45^\circ$ relative to the surface normal, we calculate an incident fluence of 6 mJ cm⁻². Using a transfer matrix algorithm for the optical absorption calculation²⁹ and literature values for the optical properties,³⁰ we find that a fraction of 25% of the incident energy is absorbed in the continuous FePt material. The hard X-ray probe-pulses with a duration of 200 fs are generated by a laser driven X-ray source, monochromatized, and focused onto the sample using a Montel optic³¹ with a convergence of approximately 0.3°. This produces a flux of approximately 10⁶ photons/s at the sample in the energy range of Cu-K α_1/α_2 X-ray characteristic line emission. To obtain the time-resolved strain from the diffracted intensity *I*, the detector images are mapped to the out-of-plane reciprocal space coordinate q_z as described previously.³² $I(q_z)$ is then fitted by a Gaussian line profile, in order to extract the position of the (002) Bragg peaks $q_{z,\text{fit}}(t)$ for each delay *t* between pump and probe pulses. Using $q_z(t) = 4\pi/c(t)$, we obtain the evolution of the average FePt lattice plane spacing *c*(*t*) in real space. The resulting strain $\varepsilon(t) = (c(t) - c_0)/c_0$, using $c_0 = c(t < 0)$, is depicted in Figs. 2(c) and 2(d).

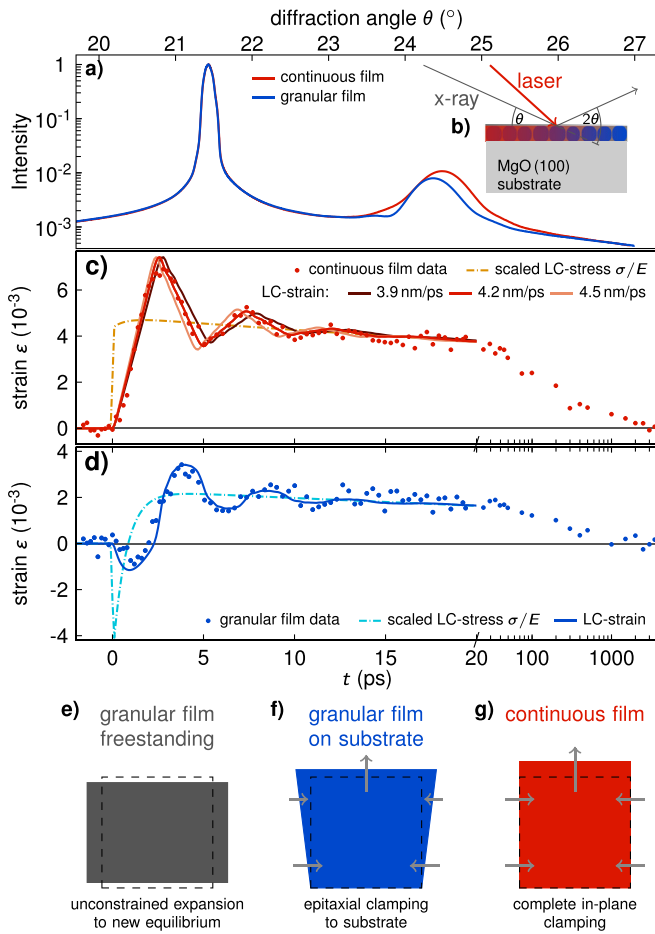


FIG. 2. X-ray diffraction and simulations: (a) Characterization of the samples using X-ray diffraction in the reflection geometry shown in the inset (b). Data points in (c) and (d) show the strain extracted from the shift of the FePt (002) Bragg peaks of the continuous and granular film in reciprocal space. Solid lines in (c) and (d) represent the transient strains that result from the applied time dependent stresses (dashed lines), in a linear chain (LC) model. The lattice dynamics in the first 10 ps of the granular film differ significantly from the strain observed in a continuous film. An initially contractive stress is required to obtain a qualitative agreement between simulation and measurement. (e)–(g) Schematic of clamping mechanisms that we believe to affect the out-of-plane expansion for the three different growth cases: (e) free-standing (f) granular film on a substrate and (g) continuous film on a substrate.

We first discuss the transient strain of the continuous FePt film [Fig. 2(c)]. An out-of-plane lattice expansion of up to 0.7% rises to its maximum within 2.8 ± 0.2 ps. Subsequently, an oscillation with a period of $T = 4.6 \pm 0.2$ ps superimposes the strain relaxation that originates from the flow of thermal energy to the substrate. From the measured T and d , we obtain the longitudinal acoustic sound velocity $v_s = 2d/T = 4.2 \pm 0.2$ nm/ps.^{33,34}

We observe a considerable out-of-plane expansion of approximately 0.4% at $t = 20$ ps for the continuous thin film after the coherent strain wave oscillations end due to repeated partial transmission into the substrate. At such large delays, the observed strain ϵ scales linearly with the quasi-thermal stress σ according to Hooke's law $\sigma = E\epsilon$. In metal films, the observed strain originates from a stress that is a superposition of the contributions from energy deposition into the electron and lattice system.^{33,35–37} In the particular case of magnetically ordered materials, additional stress

originating from the excitation of the spin system has been reported.^{10,21} Assuming thermal equilibration of these contributing subsystems, the observed strain ϵ directly indicates the transient temperature rise ΔT via $\epsilon = \alpha\Delta T$. For such a simplified analysis, we can extract an effective linear thermal expansion coefficient α , which incorporates all contributing stresses, e.g., electron and phonon pressure, magnetostriction, and the coupling of in- and out-of-plane strain by the Poisson effect by a very coarse estimation of the temperature rise. Considering the dominant contribution of the phonons to the specific heat of approximately¹⁶ $C_p = 3.5 \times 10^6$ J m⁻³ K⁻¹, we estimate from the absorbed laser fluence F_a and the film thickness d : $\Delta T = F_a/(dC) \approx 147$ K. This yields an estimate for the effective linear thermal expansion coefficient,³⁸ which is applicable only on timescales where the electron-spin-phonon system is in a quasi-equilibrium while in-plane strain propagation is still negligible: $\alpha = \epsilon/\Delta T \approx 2.7 \times 10^{-5}$ K⁻¹. The observed decaying strain for times $t > 20$ ps is attributed to a cooling of the FePt film by phonon heat transport to the insulating substrate, in agreement with previous synchrotron studies.²³ In our coarse approximation, we refer to a quasi-equilibrium, since recent theoretical developments in the modeling of time-resolved experiments that go beyond two or three temperature models indicate that such an equilibration process may take many tens of picoseconds due to mode dependent electron phonon couplings^{8,10,37} or potentially weak spin-lattice coupling.²¹

In order to further interpret the measurement on the epitaxial thin film, we simulate the results in a 1-dimensional LC model of coupled masses and springs. The simulations are carried out using the strain calculation module from the udkm1Dsim toolbox simulation package.³⁹ We calculate the response to a time-dependent expansive stress that is assumed to be homogenous across the FePt thin films motivated by the optical penetration depth³⁰ for 800 nm light in FePt of approximately 24.2 nm, which is large compared to the 9.7 nm film thickness. The dashed-dotted line in Fig. 2(c) shows the total time-dependent stress that leads to the observed transient strain, with multiple acoustic reflections shown as solid lines. It is rather close to a step function with a rising edge given by the laser pulse duration. A slight additional rise and decay can be attributed to a conversion of electronic to phononic stress and the onset of heat transport to the substrate, respectively. For convenience, we have added the simulated strain as solid lines to Fig. 2(c) assuming different longitudinal acoustic sound velocities v_s from which we can obtain the elastic constant $C_{33} = \rho v_s^2 \approx 267$ GPa using $v_s = 4.2$ nm/ps. We use the density $\rho = 15\,113$ kg/m³ of FePt calculated from atomic weights and the known unit cell dimensions of the conventional tetragonal unit cell of parameters $c = 3.72$ Å and $a = 3.85$ Å of FePt.²⁰ The derived C_{33} value lies just at the lower bound of the range of 242 – 371 GPa from theoretical considerations.^{11–13} It agrees well with the observed reduction of the elastic constant of FePt specimen from 309 to about 250 GPa, when the thickness is less than 40 nm.¹⁷ The temperature dependence of the elastic constants observed under equilibrium heating¹⁸ supports an even further decrease in the transient bulk modulus resulting from a laser-induced temperature increase. The surprisingly small $v_s = 2.2$ nm/ps reported for the free standing

grains¹⁰ might be due to a missing factor of 2 since for spheres, the expected period $T = d/v_s$ must be calculated using the diameter d of the laser excited particles instead of their radius.

Now, we discuss the dynamics in our nano-granular film. The oscillation period is nearly identical to the continuous film, as expected for the same layer thickness. The in-plane dynamics of the granular film occur with a similar period because the average grain size equals the thickness. Its out-of-plane contraction within the first 2.5 ps [Fig. 2(d)] confirms the ultrafast contractive stress contribution that was reported for the free-standing granular film.¹⁰ The contractive stress component was shown to originate from the release of magnetostriction due to the transient demagnetization of the FePt.¹⁰ The timescale of the demagnetization varies depending on the experimental conditions but is usually fitted by an exponential decay with time constants smaller than 0.5 ps.^{10,26,27} The magnetization recovers within several tens of picoseconds, depending on the excitation fluence.^{10,26} For larger time delays ($t > 2.5$ ps), we definitely observe a long-lasting lattice expansion, which has only about half the amplitude of the continuous film. The contractive stress driven by spin-excitations is still operative due to the slow remagnetization, but the phonon-driven heat expansion prevails. As we argue below, the crossover from compressive to tensile strain is due to partial constraints to the in-plane motion of the nanograins. The contraction observed in the free standing film is thus probably stopped as soon as the in-plane grain expansion is inhibited by the epitaxial pinning to the MgO substrate and the surrounding carbon matrix, which is also pinned to the substrate. In the case of the continuous epitaxial film, such in-plane constraints completely inhibit the compressive strain at early delays.

For the epitaxial continuous film, the 1D LC model is an excellent approximation for the first 20 ps, since in-plane motion is prohibited by symmetry. In the nano-granular sample, this symmetry is broken and various anisotropic driving stresses can occur so that a modeling of the three-dimensional response of particles with anisotropic elastic properties embedded in a carbon matrix would be required. The inhomogeneous size distribution with unknown coupling strength to the substrate further challenges *ab-initio* treatment. Here, we analyze the strain response of the FePt granular sample grown on a substrate, because it connects the previous research on free-standing nanograins¹⁰ and epitaxial thin films²³ and since it is the relevant geometry used in HAMR media. For a simplified simulation of the observed out-of-plane strain, we assume the effective out-of-plane stress shown in Fig. 2(d) as a dashed-dotted line, which includes contributions from an in-plane expansion that leads to an out-of-plane contractive stress via Poisson's ratio. We speculate that the crossover from a contractive to an expansive out-of-plane stress within about 1 ps is due to the fact that the in-plane expansion concomitant with the out-of-plane contraction is hindered by epitaxial clamping to the substrate and the carbon matrix. This contribution of the Poisson effect adds to the out-of-plane contraction driven by ultrafast spin disordering.¹⁰

Figures 2(e)–2(g) schematically show our current understanding of the pronounced differences for free-standing

grains vs. continuous epitaxial films of FePt, with nano-granular films on a substrate as an intermediate case. While the nearly free-standing grains, which are more loosely embedded in a carbon matrix on a TEM grid, can contract out-of-plane because they can expand in-plane, the continuous film cannot expand in-plane. This suppresses the contraction out-of-plane and an expansion due to electron and phonon stresses prevails. For the nano-granular film on the substrate, the in-plane expansion is still somewhat suppressed due to the carbon matrix and due to epitaxial strain resulting from the pinning to the substrate.

In conclusion, we have shown that laser-excited FePt in the L1₀ phase essentially expands out-of-plane, if the continuous film or the nano-grains are epitaxially attached to a substrate. From the observed strain-wave oscillations, we obtain the out-of-plane sound velocity and thus the elastic constant C_{33} , well in line with the reported decrease for films of few nm thickness.¹⁷ Our experiments showcase the capabilities of table-top UXR to monitor transient stresses via the resulting coherent strain waves. The subpicosecond time-resolution of the experiments reveal a markedly different response of the granular sample compared to the continuous film. This proves the relevance of different balances of the in-plane stresses for the out-of-plane lattice dynamics. Few previous experimental studies assume that the related Poisson effect enhances the amplitude of ultrafast generated strain in continuous films,^{21,38,40} however, an unambiguous general proof for this enhancement is so far missing.

The complexity of the anisotropic nanogranular samples calls for modeling approaches that go beyond harmonic oscillator models^{8,16} or the 1D approximation that is frequently applied in laser-excited bulk materials or continuous thin films since the seminal work of Thomson *et al.*⁴¹ We envision that time-resolved studies of various properties of nanoparticles could be cross-fertilized by the development of three-dimensional model calculations since they are often intricately linked to the lattice via changes in their band structure.

We acknowledge the BMBF for the financial support via 05K16IPA and the DFG via BA 2281/8-1 and BA 2281/11-1.

¹S. Wicht, S. Wee, O. Hellwig, V. Mehta, S. Jain, D. Weller, and B. Rellinghaus, *J. Appl. Phys.* **119**, 115301 (2016).

²O. Mosendz, S. Pisana, J. Reiner, B. Stipe, and D. Weller, *J. Appl. Phys.* **111**, 07B729 (2012).

³D. Weller, A. Moser, L. Folks, M. Best, W. Lee, M. Toney, M. Schwickert, J.-U. Thiele, and M. Doerner, *IEEE Trans. Magn.* **36**, 10 (2000).

⁴D. Weller, O. Mosendz, G. Parker, S. Pisana, and T. S. Santos, *Phys. Status Solidi A* **210**, 1245 (2013).

⁵D. Weller, G. Parker, O. Mosendz, A. Lyberatos, D. Mitin, N. Y. Safonova, and M. Albrecht, *J. Vac. Sci. Technol.*, **B 34**, 060801 (2016).

⁶O. Hovorka, S. Devos, Q. Coopman, W. J. Fan, C. J. Aas, R. F. L. Evans, X. Chen, G. Ju, and R. W. Chantrell, *Appl. Phys. Lett.* **101**, 052406 (2012).

⁷S. Pisana, S. Jain, J. Reiner, G. Parker, C. Poon, O. Hellwig, and B. Stipe, *Appl. Phys. Lett.* **104**, 162407 (2014).

⁸P. Maldonado, K. Carva, M. Flammer, and P. M. Oppeneer, *Phys. Rev. B* **96**, 174439 (2017).

⁹N. Kazantseva, D. Hinzke, U. Nowak, R. W. Chantrell, U. Atxitia, and O. Chubykalo-Fesenko, *Phys. Rev. B* **77**, 184428 (2008).

¹⁰A. H. Reid, X. Shen, P. Maldonado, T. Chase, E. Jal, P. W. Granitzka, K. Carva, R. K. Li, J. Li, L. Wu, T. Vecchione, T. Liu, Z. Chen, D. J. Hgley,

- N. Hartmann, R. Coffee, J. Wu, G. L. Dakovski, W. F. Schlotter, H. Ohldag, Y. K. Takahashi, V. Mehta, O. Hellwig, A. Fry, Y. Zhu, J. Cao, E. E. Fullerton, J. Stöhr, P. M. Oppeneer, X. J. Wang, and H. A. Dürr, *Nat. Commun.* **9**, 388 (2018).
- ¹¹J. Kim, Y. Koo, and B.-J. Lee, *J. Mater. Res.* **21**, 199 (2006).
- ¹²M. Müller, P. Erhart, and K. Albe, *J. Phys.: Condens. Matter* **19**, 326220 (2007).
- ¹³N. Zotov and A. Ludwig, *Intermetallics* **16**, 113 (2008).
- ¹⁴A. Chernyshov, D. Treves, T. Le, F. Zong, A. Ajan, and R. Acharya, *J. Appl. Phys.* **115**, 17B735 (2014).
- ¹⁵A. Giri, S. H. Wee, S. Jain, O. Hellwig, and P. E. Hopkins, *Sci. Rep.* **6**, 32077 (2016).
- ¹⁶J. Kimling, J. Kimling, R. Wilson, B. Hebler, M. Albrecht, and D. G. Cahill, *Phys. Rev. B* **90**, 224408 (2014).
- ¹⁷N. Nakamura, A. Uranishi, M. Wakita, H. Ogi, M. Hirao, and M. Nishiyama, *Appl. Phys. Lett.* **98**, 101911 (2011).
- ¹⁸N. Nakamura, N. Yoshimura, H. Ogi, and M. Hirao, *J. Appl. Phys.* **114**, 093506 (2013).
- ¹⁹R. Nicula, O. Crisan, A. Crisan, I. Mercioniu, M. Stir, and F. Vasiliu, *J. Alloys Compd.* **622**, 865 (2015).
- ²⁰Y. Tsunoda and H. Kobayashi, *J. Magn. Magn. Mater.* **272**, 776 (2004).
- ²¹A. von Reppert, J. Pudell, A. Koc, M. Reinhardt, W. Leitenberger, K. Dumesnil, F. Zamponi, and M. Bargheer, *Struct. Dyn.* **3**, 054302 (2016).
- ²²A. Von Reppert, R. Sarhan, F. Stete, J. Pudell, N. Del Fatti, A. Crut, J. Koetz, F. Liebig, C. Prietzel, and M. Bargheer, *J. Phys. Chem. C* **120**, 28894 (2016).
- ²³D. Xu, C. Sun, D. Brewes, S.-W. Han, P. Ho, J. Chen, S. Heald, X. Zhang, and G. Chow, *J. Appl. Phys.* **115**, 243907 (2014).
- ²⁴M. Reinhardt and W. Leitenberger, *J. Large-Scale Res. Facil.* **2**, 89 (2016).
- ²⁵P. A. Kienzie, K. V. O'Donovan, J. F. Ankner, N. Berk, and C. Majkrzak, "NCNR Reflectometry Software," (2006).
- ²⁶J. Mendil, P. Nieves, O. Chubykalo-Fesenko, J. Walowski, T. Santos, S. Pisana, and M. Münzenberg, *Sci. Rep.* **4**, 3980 (2014).
- ²⁷T. Shima, K. Takanashi, Y. K. Takahashi, and K. Hono, *Appl. Phys. Lett.* **81**, 1050 (2002).
- ²⁸D. Schick, A. Bojahr, M. Herzog, C. V. K. Schmising, R. Shayduk, W. Leitenberger, P. Gaal, and M. Bargheer, *Rev. Sci. Instrum.* **83**, 025104 (2012).
- ²⁹L. Le Guyader, A. Kleibert, F. Nolting, L. Joly, P. Derlet, R. Pisarev, A. Kirilyuk, T. Rasing, and A. Kimel, *Phys. Rev. B* **87**, 054437 (2013).
- ³⁰Z. H. Cen, B. X. Xu, J. F. Hu, J. M. Li, K. M. Cher, Y. T. Toh, K. D. Ye, and J. Zhang, *Opt. Express* **21**, 9906 (2013).
- ³¹M. Bargheer, N. Zhavoronkov, R. Bruch, H. Legall, H. Stiel, M. Woerner, and T. Elsaesser, *Appl. Phys. B* **80**, 715 (2005).
- ³²D. Schick, R. Shayduk, A. Bojahr, M. Herzog, C. von Korff Schmising, P. Gaal, and M. Bargheer, *J. Appl. Crystallogr.* **46**, 1372 (2013).
- ³³M. Nicoul, U. Shymanovich, A. Tarasevitch, D. von der Linde, and K. Sokolowski-Tinten, *Appl. Phys. Lett.* **98**, 191902 (2011).
- ³⁴D. Schick, M. Herzog, A. Bojahr, W. Leitenberger, A. Hertwig, R. Shayduk, and M. Bargheer, *Struct. Dyn.* **1**, 064501 (2014).
- ³⁵S. Nie, X. Wang, H. Park, R. Clinite, and J. Cao, *Phys. Rev. Lett.* **96**, 25901 (2006).
- ³⁶K. Sokolowski-Tinten, X. Shen, Q. Zheng, T. Chase, R. Coffee, M. Jerman, R. K. Li, M. Ligges, I. Makasyuk, M. Mo, A. H. Reid, B. Rethfeld, T. Vecchione, S. P. Weathersby, H. A. Dürr, and X. J. Wang, *Struct. Dyn.* **4**, 054501 (2017).
- ³⁷T. Henighan, M. Trigo, S. Bonetti, P. Granitzka, D. Higley, Z. Chen, M. P. Jiang, R. Kukreja, A. Gray, A. H. Reid, E. Jal, M. C. Hoffmann, M. Kozina, S. Song, M. Chollet, D. Zhu, P. F. Xu, J. Jeong, K. Carva, P. Maldonado, P. M. Oppeneer, M. G. Samant, S. S. P. Parkin, D. A. Reis, and H. A. Dürr, *Phys. Rev. B* **93**, 220301 (2016).
- ³⁸J. Pudell, A. A. Maznev, M. Herzog, M. Kronseder, C. H. Back, G. Malinowski, A. von Reppert, and M. Bargheer, *Nat. Commun.* **9**, 3335 (2016).
- ³⁹D. Schick, A. Bojahr, M. Herzog, C. von Korff Schmising, R. Shayduk, and M. Bargheer, *Comput. Phys. Commun.* **185**, 651 (2014).
- ⁴⁰H. J. Lee, J. Workman, J. S. Wark, R. D. Averitt, A. J. Taylor, J. Roberts, Q. McCulloch, D. E. Hof, N. Hur, S.-W. Cheong, and D. J. Funk, *Phys. Rev. B* **77**, 132301 (2008).
- ⁴¹C. Thomsen, H. T. Grahn, H. J. Maris, and J. Tauc, *Phys. Rev. B* **34**, 4129 (1986).